

One-to-One correspondence of soft and hard Pomeron with the CDP of the gluon density at low x

G.R.Boroun*

Department of Physics, Razi University, Kermanshah 67149, Iran
(Dated: January 5, 2023)

The correspondence between the gluon density behavior of the color dipole picture and the two-Pomeron approach at low x deep inelastic scattering is considered. For photon virtualities of $Q^2 \gtrsim 10 \text{ GeV}^2$, the results for the parametrization and CDP models are defined by the CDP asymptotic limit and are compatible with the soft and hard-Pomeron approach. These results show that the hard-Pomeron trajectory does not guarantee converging towards the asymptotic representation at low and large Q^2 ($Q^2 \lesssim 100 \text{ GeV}^2$) values in a wide range of the virtual-photon-proton energy squared. The gluon distributions can be obtained directly in terms of the proton structure functions and the running coupling and compared with the results from the GJR and MSTW parametrizations.

1. Introduction

Sakurai and Schildknecht in 1972 [1] starting points on the color dipole picture (CDP) which provides a convenient description of deep inelastic scattering (DIS) at low x [2-5]. In this picture, the DIS cross section is factorized into a light-cone wave function, as the virtual photon fluctuates into the $q\bar{q}$ pair. This split is defined as a convolution of the infinite momentum frame wave function with the pQCD calculable coefficient functions. Then the $q\bar{q}$ pair interacts with the gluon field in the nucleon as a gauge-invariant color-dipole interaction. In this interaction the $q\bar{q}$ lifetime is about $1/x$ times longer than time of interaction photon with proton [6]. At low values of the Bjorken variable $x \equiv x_{\text{Bj}} \simeq Q^2/W^2$, DIS of electrons on protons defined by the processes splitting of the photon into on-shell quark-antiquark states and interaction these states on the proton. Here Q^2 refers to the photon virtuality and W to the photon-proton center-of-mass energy. In the transverse position space, the photoabsorption cross section at low values of x is defined by the square of the photon wave function and the dipole cross section as [2,5,7]

$$\sigma_{\gamma_{L,T}^*}(W^2, Q^2) = \int dz \int d^2\mathbf{r}_\perp |\Psi_{L,T}(\mathbf{r}_\perp, z(1-z), Q^2)|^2 \times \sigma_{(q\bar{q})p}(\mathbf{r}_\perp, z(1-z), W^2). \quad (1)$$

The variable z determines the direction of the three-momentum of the quark due to the photon direction and $|\Psi_{L,T}|^2$ describes the probability of the occurrence of a quark-antiquark fluctuation with respect to the polarization direction. The dipole cross section, related to the imaginary part of the $(q\bar{q})p$ forward scattering amplitude. The dipole cross section depends on the center-of-mass

energy, W , of the $(q\bar{q})p$ scattering process, as this implies that the structure function reads

$$F_2(x, Q^2) \simeq \frac{Q^2}{4\pi^2\alpha_{EM}} [\sigma_{\gamma_{LP}^*}(W^2, Q^2) + \sigma_{\gamma_{TP}^*}(W^2, Q^2)]. \quad (2)$$

Indeed, the structure function becomes a function of the single variable W^2 . In Refs.[5,7] we observe that the experimental data corresponding to $1/W^2 \leq 10^{-3}$ lie on a single line in the relevant range of $x < 0.1$.

A new parameterization of the proton structure function which describes fairly well the available experimental data on the reduced cross section at low values of x described in Ref.[8,9]. In Ref.[8] authors use an updated version of the global parameterization of the ZEUS data [10] for the proton structure function made by authors in Ref.[11]. Authors modified the fit in two important aspects of the sieve algorithm [12] which minimizes the squared Lorentzian [9,11] and obtained free parameters according to the renormalized χ^2_{min} per degree of freedom whose contribution was 193.19. Analytical expression successfully reproduces the known experimental data for $F_2(x, Q^2)$ in a wide range of Q^2 values, $0.11 \leq Q^2 \leq 1200 \text{ GeV}^2$, and Bjorken x range, $10^{-6} \leq x \leq 0.0494$. Then the authors in Ref.[9] completed the parameterization method to fit all of the HERA DIS data on $F_2(x, Q^2)$ at low values of x that satisfies a saturated Froissart bound behavior. The parameterization of the proton structure function [9] is in full accordance with the Froissart predictions on the available experimental data in a range of the kinematical variables x and Q^2 , $x \leq 0.1$ and $0.15 < Q^2 < 3000 \text{ GeV}^2$. This paper is organized as follows. In the next section, the theoretical formalism is presented, including the parameterization of $F_2(x, Q^2)$ and the color dipole picture. In section 3, we present a detailed numerical analysis and our main results for the CDP, parametrization and Regge models. In the last section we summarize our main conclusions and remarks.

*Electronic address: boroun@razi.ac.ir

2. Theoretical formalism

In view of low values of $x \cong Q^2/W^2 < 0.1$, the transverse $F_2(x, Q^2)$ and longitudinal $F_L(x, Q^2)$ structure functions are expressed via the gluon distribution $xg(x, Q^2)$ ($k = 2, L$) as the approximation relation reads

$$F_k(x, Q^2) \simeq \langle e^2 \rangle C_{k,g}(x, Q^2) \otimes xg(x, Q^2). \quad (3)$$

The symbol \otimes denotes a convolution according to the usual prescription, $f(x) \otimes g(x) = \int_x^1 \frac{dy}{y} f(y) g(\frac{x}{y})$. Here $\langle e^k \rangle$ is the average of the charge e^k for the active quark flavors, $\langle e^k \rangle = n_f^{-1} \sum_{i=1}^{n_f} e_i^k$ with n_f as the number of considered flavors and $C_{k,g}$ are the common Wilson coefficient functions [13]. At leading order (LO) approximation, the longitudinal structure function becomes proportional to the gluon density at a rescaled value x/ξ_L [14,15] as

$$F_L(\xi_L x, Q^2) = \frac{\alpha_s(Q^2)}{3\pi} \sum e_q^2 xg(x, Q^2), \quad (4)$$

where the rescaling factor in the above equation has the preferred values of $\xi_L \cong 0.40$ and $\alpha_s(Q^2)$ is the running coupling at the leading order (LO, $n=0$) and the next-to leading order (NLO, $n=1$) approximations by the following form, respectively

$$\alpha_s(Q^2) = \frac{1}{bt} \left[1 - n \frac{b' \ln t}{bt} \right], \quad (5)$$

with $b = \frac{33-2n_f}{12\pi}$ and $b' = \frac{153-19n_f}{2\pi(33-2n_f)}$, where $t = \ln(\frac{Q^2}{\Lambda_{QCD}^2})$. The running of the coupling constant α_s is determined by the renormalization group equation $Q^2 \frac{\partial \alpha_s}{\partial Q^2} = \beta(\alpha_s)$, where the β function in QCD has the perturbative expansion [16-17]

$$\beta(\alpha_s) = -\alpha_s \sum_{n=0}^{\infty} \beta_n \left(\frac{\alpha_s}{4\pi} \right)^{(n+1)}$$

where $\beta_0 = 4\pi b$ and $\beta_1 = 16\pi^2 b b'$. In Ref.[18], the author has discussed that the running coupling of a generic field theory can be described through a separable differential equation involving the corresponding β -function. Only the first loop order can be solved analytically in terms of well-known functions. For further loop orders the running coupling leads to transcendental equations, where by applying an optimal Padé approximant on the β -function, it leads to generalizations of Lambert's equation. Its solution is presented in terms of a power series, as at low Q^2 values, the appropriate NLO transcendental equation for α_s should be used.

The evolution equation of the singlet distribution function at LO analysis at low x is given by

$$\frac{\partial \Sigma(x, Q^2)}{\partial \ln Q^2} = \frac{\alpha_s(Q^2)}{2\pi} P_{qg}(\alpha_s, x) \otimes xg(x, Q^2), \quad (6)$$

where $P_{qg}(\alpha_s, x)$ is the quark-gluon splitting function. Σ is the singlet density and for $n_f = 4$ reads

$$F_2(x, Q^2) = \frac{1}{4} \sum e_q^2 x \Sigma(x, Q^2) = \frac{5}{18} x \Sigma(x, Q^2). \quad (7)$$

A similar relation for the derivative of $F_2(x, Q^2)$ with respect to $\ln Q^2$ at low x is determined by the authors in Refs.[19-22] as

$$\frac{\partial F_2(\xi_2 x, Q^2)}{\partial \ln Q^2} = \frac{\alpha_s(Q^2)}{3\pi} \sum e_q^2 xg(x, Q^2), \quad (8)$$

where the rescaling factor for $F_2(x, Q^2)$ has the preferred values of $\xi_2 \cong 0.50$. Combining Eqs.(4) and (8), one can calculate the longitudinal structure function by the derivative of the structure function at a rescaled value ηx as

$$F_L(x, Q^2) = \frac{\partial F_2(\eta x, Q^2)}{\partial \ln Q^2}, \quad (9)$$

where $\eta = \frac{\xi_2}{\xi_L} \simeq 1.25$. In CDP, the ratio of structure functions is dependent on the kinematic variable $\rho \equiv \rho(x, Q^2)$ by the following form

$$\frac{F_L(x, Q^2)}{F_2(x, Q^2)} = \frac{1}{1 + 2\rho}. \quad (10)$$

The parameter ρ is associated with the enhanced transverse size of $q\bar{q}$ fluctuations originating from the difference in the photon wave functions as

$$\frac{\sigma_{\gamma_L^*}(W^2, Q^2)}{\sigma_{\gamma_T^*}(W^2, Q^2)} = \frac{1}{2\rho}. \quad (11)$$

With imposing consistency between the CDP and the pQCD, the authors in Refs.[5,7,23] obtained the gluon distribution function by expressing the longitudinal structure function in terms of $F_2(x, Q^2)$ as [7]

$$\alpha_s(Q^2) xg(x, Q^2) = \frac{3\pi}{\sum e_q^2 (2\rho + 1)} F_2(\xi_L x, Q^2). \quad (12)$$

The above equation (i.e., Eq.(12)) can be used to study the behavior of $\alpha_s(Q^2) xg(x, Q^2)$ due to the proton structure function.

• Color Dipole Model

In CDP [5,7,23], at sufficiently large Q^2 for $x < 0.1$, the structure function depends on the single variable W^2

$$F_2(x, Q^2) = F_2(W^2 = \frac{Q^2}{x}), \quad (13)$$

which is consistent with the experimental data with an eye-ball fit by the form

$$F_2(W^2) = f_2 \left(\frac{W^2}{1 \text{ GeV}^2} \right)^{C_2}, \quad (14)$$

with $f_2 = 0.063$ and $C_2 = 0.29$. In this picture, the known expression for $\alpha_s(Q^2)xg(x, Q^2)$ (with respect to Eqs.(12) and (14)) reads as follows

$$\alpha_s(Q^2)xg(x, Q^2) = \frac{3\pi}{(2\rho+1)\sum e_q^2} \frac{f_2}{\xi_L^{C_2}} \left(\frac{W^2}{1\text{GeV}^2}\right)^{C_2}, \quad (15)$$

where $\rho = 4/3$ and $\sum e_q^2 = 10/9$ for four active flavors.

• Parametrization Model

The proton structure function is parametrized with a global fit function [9] with a combined fit to the H1 and ZEUS Collaboration data for $F_2(x, Q^2)$ at $0.15 < Q^2 < 3000 \text{ GeV}^2$ and $x < 0.01$ takes the form

$$F_2(x, Q^2) = D(Q^2)(1-x)^n \sum_{m=0}^2 A_m(Q^2) L^m(x, Q^2), \quad (16)$$

where

$$\begin{aligned} D(Q^2) &= \frac{Q^2(Q^2 + \lambda M^2)}{(Q^2 + M^2)^2}, \\ A_0(Q^2) &= a_{00} + a_{01} L_2(Q^2), \\ A_i(Q^2) &= \sum_{k=0}^2 a_{ik} L_2(Q^2)^k, \quad i = (1, 2), \\ L(Q^2, x) &= \ln \frac{1}{x} + \ln \frac{Q^2}{Q^2 + \mu^2}, \\ L_2(Q^2) &= \ln \frac{Q^2 + \mu^2}{\mu^2}, \end{aligned} \quad (17)$$

and the effective parameters are defined in Table I. Note that the results of using the parametrization method can be found recently in Refs.[24-26]. In this picture, the known expression for $\alpha_s(Q^2)xg(x, Q^2)$ (with respect to Eqs.(12) and (16)) reads as follows

$$\alpha_s(Q^2)xg(x, Q^2) = \frac{3\pi}{(2\rho+1)\sum e_q^2} D(Q^2)(1-\xi_L x)^n \sum_{m=0}^2 A_m(Q^2) L^m(\xi_L x, Q^2). \quad (18)$$

• Two – Pomeron Model

HERA has shows that the $\sigma^{\gamma^* p}$ rapid rise with W^2 as an effective power

$$\sigma^{\gamma^* p} \sim F(Q^2)(W^2)^{\lambda(Q^2)}, \quad (19)$$

where the power $\lambda(Q^2)$ has been extracted by H1 Collaboration in Ref.[27]. The effective-power behavior of the proton structure function at low x corresponds to

$$F_2(x, Q^2) \sim f(Q^2)x^{-\lambda(Q^2)}. \quad (20)$$

Rather, the authors in Ref.[28] show that one should parametrize the data with a sum of fixed powers of x in the two-Pomeron model as

$$\begin{aligned} F_2(x, Q^2) &\sim \sum_{i=0,1} f_i(Q^2)x^{-\epsilon_i} \\ &= F_2^{\text{hard}} + F_2^{\text{soft}}, \end{aligned} \quad (21)$$

where the $i = 0$ term is hard-Pomeron exchange and $i = 1$ term is soft-Pomeron exchange. The authors in Ref.[28] showed that a very good fit to data (for $Q^2 = 0$ to 5000 GeV^2) was provided by the economical parameterization as

$$\begin{aligned} f_0(Q^2) &= \frac{A_0(Q^2)^{1+\epsilon_0}}{(1+Q^2/Q_0^2)^{1+\epsilon_0/2}}, \\ f_1(Q^2) &= \frac{A_1(Q^2)^{1+\epsilon_1}}{(1+Q^2/Q_1^2)^{1+\epsilon_1}}, \end{aligned} \quad (22)$$

where $\epsilon_0 = 0.452$, $\epsilon_1 = 0.0667$, $A_0 = 0.00151$, $A_1 = 0.658$, $Q_0^2 = 7.85$ and $Q_1^2 = 0.658$.

In this model, the known expression for $\alpha_s(Q^2)xg(x, Q^2)$ (with respect to Eqs.(12) and (21)) reads as follows

$$\begin{aligned} \alpha_s(Q^2)xg(x, Q^2) &= \frac{3\pi}{(2\rho+1)\sum e_q^2} [f_0(Q^2)(\xi_L x)^{-\epsilon_0} \\ &\quad + f_1(Q^2)(\xi_L x)^{-\epsilon_1}]. \end{aligned} \quad (23)$$

• Tensor – Pomeron Model

Recently, in Ref.[29], the validity of the CDP with respect to the tensor-Pomeron model [30] for photon virtualities of $Q^2 \gtrsim 20 \text{ GeV}^2$ is considered. Consistency of the models has shown that the CDP with the perturbative QCD (pQCD) improved parton model at low x . Authors in Ref.[30] applied the tensor-Pomeron model to low- x deep-inelastic lepton-nucleon scattering and photoproduction due to the center-of-mass energies in the range $6 - 318 \text{ GeV}$ and $Q^2 \lesssim 50 \text{ GeV}^2$. The hadronic high-energy reactions defined with respect to the two-Pomeron-plus-Reggeon approach in Ref.[30]. The virtual Compton amplitude in the tensor-Pomeron approach for large W^2 is defined by the exchange of the two Pomerons, $\mathbb{P}0$ and $\mathbb{P}1$, plus the $f_2 R$ reggeon. Therefore the proton structure function, in the tensor-Pomeron model, leads

$$\begin{aligned} F_2(W^2, Q^2) &= \frac{Q^2}{\pi} (1-x)[1+2\delta((W^2, Q^2))]^{-1} \frac{W^2 - m_p^2}{W^2} \\ &\quad 3 \sum_{j=0,1,2} \hat{b}_j(Q^2) \beta_{jpp}(W^2 \tilde{\alpha}'_j)^{\epsilon_j} \cos\left(\frac{\pi}{2} \epsilon_j\right) \\ &\quad \left[1 + \frac{2Q^2}{W^2 - m_p^2} + \frac{Q^2(Q^2 + m_p^2)}{(W^2 - m_p^2)^2}\right], \end{aligned} \quad (24)$$

where

$$\delta(W^2, Q^2) = \frac{2m_p^2 Q^2}{(W^2 + Q^2 - m_p^2)^2}.$$

The parameters of the tensor-Pomeron approach with hard and soft Pomeron and $f_2 R$ reggeon exchange are

$$\text{Soft :} \quad \alpha'_1 = \tilde{\alpha}'_1 = 0.25 \text{ GeV}^{-2}, \quad \varepsilon_1 = \alpha_1(0) - 1, \\ \varepsilon_1 = 0.0935^{(+76)}_{(-64)},$$

$$\text{Hard :} \quad \alpha'_0 = \tilde{\alpha}'_0 = 0.25 \text{ GeV}^{-2}, \quad \varepsilon_0 = \alpha_0(0) - 1, \\ \varepsilon_0 = 0.3008^{(+73)}_{(-84)},$$

$$\text{Reggeon :} \quad \alpha'_2 = \tilde{\alpha}'_2 = 0.90 \text{ GeV}^{-2}, \quad \alpha_2(0) = 0.485^{(+88)}_{(-90)},$$

where $\beta_{0pp} = \beta_{1pp} = 1.87 \text{ GeV}^{-1}$, $\beta_{2pp} = 3.68 \text{ GeV}^{-1}$ and $m_p = 0.938 \text{ GeV}$. The values of coupling functions, $\hat{b}_j(Q^2)$, obtained in the fit HERA DIS and photoproduction data read

$$\begin{aligned} \hat{b}_0(10 \text{ GeV}^2) &= \exp(-5.669^{(+99)}_{(-101)}) \text{ GeV}^{-1} \\ \hat{b}_0(50 \text{ GeV}^2) &= \exp(-6.899^{(+78)}_{(-80)}) \text{ GeV}^{-1} \\ \hat{b}_1(10 \text{ GeV}^2) &= \exp(-4.668(70)) \text{ GeV}^{-1} \\ \hat{b}_1(50 \text{ GeV}^2) &= \exp(-7.870(29)) \text{ GeV}^{-1} \end{aligned}$$

and

$$\begin{aligned} \hat{b}_2(Q^2) &= c_2 \exp(-Q^2/d_2) \\ c_2 &= \exp(-0.38^{(+36)}_{(-35)}) \text{ GeV}^{-1} \\ d_2 &= \exp(-1.35^{(+34)}_{(-35)}) \text{ GeV}^{-2}, \end{aligned}$$

where the uncertainties indicated in the above brackets are determined using the MINOS algorithm. Therefore, the gluon distribution multiplied by the running coupling (with respect to Eqs.(12) and (24)) reads

$$\begin{aligned} \alpha_s(Q^2) x g(x, Q^2) &= \frac{3\pi}{(2\rho+1) \sum e_q^2} \frac{Q^2}{\pi} (1 - \xi_L x) \\ &\quad 3[1 + 2\delta((W^2, Q^2))]^{-1} \frac{W^2 - m_p^2}{W^2} \\ &\quad \sum_{j=0,1,2} \hat{b}_j(Q^2) \beta_{jpp} (W^2 \tilde{\alpha}'_j)^{\varepsilon_j} \cos\left(\frac{\pi}{2} \varepsilon_j\right) \\ &\quad \left[1 + \frac{2Q^2}{W^2 - m_p^2} + \frac{Q^2(Q^2 + m_p^2)}{(W^2 - m_p^2)^2}\right]. \quad (25) \end{aligned}$$

In the following, we employ the parameterization of the proton structure function, two and tensor-Pomeron models in CDP and consider the behavior of the $\alpha_s(Q^2) x g(x, Q^2)$ into the center-of-mass energy W , due to Eqs.(15, 18, 23) and (25), in the next section.

3. Results and discussions

We have calculated the W^2 -dependence, at low x , of $\alpha_s(Q^2) x g(x, Q^2)$ according to the CDP and compared with the parametrization and Pomeron models. Results of calculations and comparisons are presented in Figs. 1 up to 4. In Fig.1 we compared the behavior of the gluon

distribution with respect to the CDP asymptotic limit (Eq.(15)) and the parametrization of the proton structure function (Eq.(18)) for $1 \text{ GeV}^2 \leq Q^2 \leq 100 \text{ GeV}^2$ in a wide range of W^2 . In this figure (i.e., Fig.1) we observe that the parametrization model results converge towards the CDP asymptotic limit for $Q^2 \gtrsim 10 \text{ GeV}^2$.

In Fig.2 we compared the results in Fig.1 with respect to the CDP results at any Q^2 value. These results are based on $F_2(\xi_L x, Q^2)$ according to (12) and are comparable with the CDP asymptotic limit and the parametrization model at moderate and large Q^2 values.

In Fig.3, we compared the Regge behavior with the

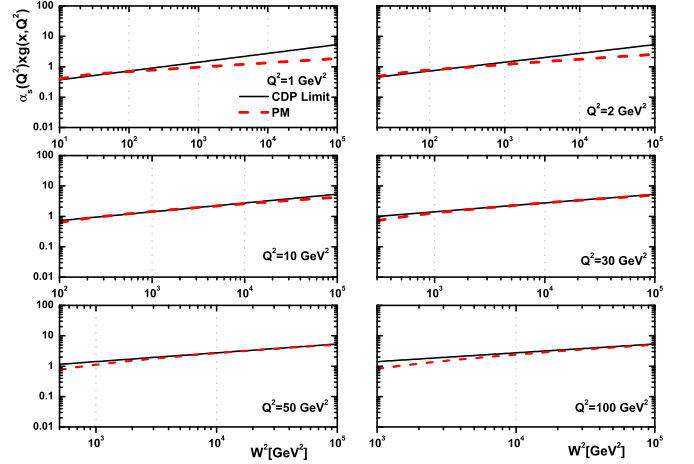


FIG. 1: $\alpha_s(Q^2) x g(x, Q^2)$ as a function of W^2 for various values of Q^2 in the CDP asymptotic limit (Eq.15)(solid curve) and parametrization model (PM, Eq.18)(dashed curve).

parametrization model and the CDP predictions. The parametrization model is comparable with the Regge behavior at low and large Q^2 values and it is comparable with CDP at moderate and high Q^2 values. In this figure (i.e., Fig.3), the Regge behavior is defined into the soft and hard Pomeron behaviors. The behavior of the two-Pomeron approach converge towards the CDP and parametrization models at $Q^2 \gtrsim 10 \text{ GeV}^2$. Consistency between results for moderate and large Q^2 values shows that two-Pomeron approach leads to the CDP asymptotic limit where it is free of Q^2 parameters. This indicates that the Regge model must have at least two parameters or more to match the models. In Ref.[30] two-Pomeron-plus-Reggeon approach fitted to the experimental data on the deep-inelastic lepton-nucleon scattering at low values of x and consistency with the CDP is introduced in Ref.[29].

In fact, we have shown that in order to converge the CDP results with the Regge theory, it is necessary to introduce the Regge theory with two-Pomeron approach. In this connection, we plot $\alpha_s(Q^2) x g(x, Q^2)$ according

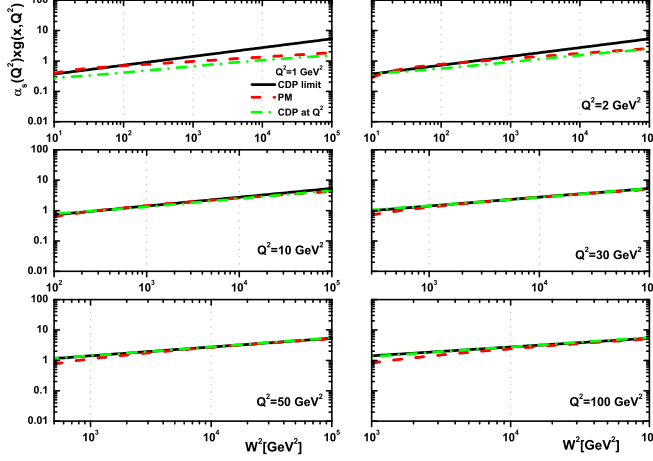


FIG. 2: Same as Fig.1 but based on (Eq.12)(dashed-dot curve).

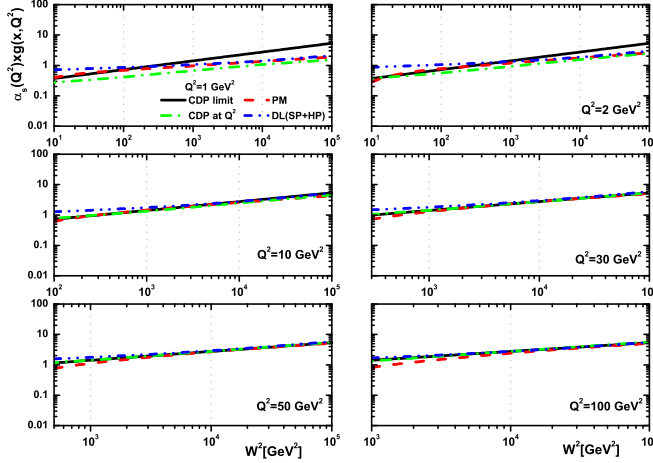


FIG. 3: Same as Fig.2, and compared with soft and hard Pomeron model (SP+HP,Eq.23) (dashed-dot-dot curve).

to Eqs.(12,15) and (18) and compared the Regge theory with respect to the only hard-Pomeron trajectory due to Eq.(23). In Fig.4, we observe that the hard-Pomeron approach result do not converge with the CDP and parametrization models for $1 \text{ GeV}^2 \leq Q^2 \leq 100 \text{ GeV}^2$ in a wide range of W^2 . Indeed, the results obtained by employing the CDP representation of the experimental data of the proton structure function in the pQCD improved parton model do not support the necessity of modifications by single (hard) Pomeron effects at $Q^2 \leq 100 \text{ GeV}^2$. We can observe that there is asymptotically agree between the parametrization and hard-

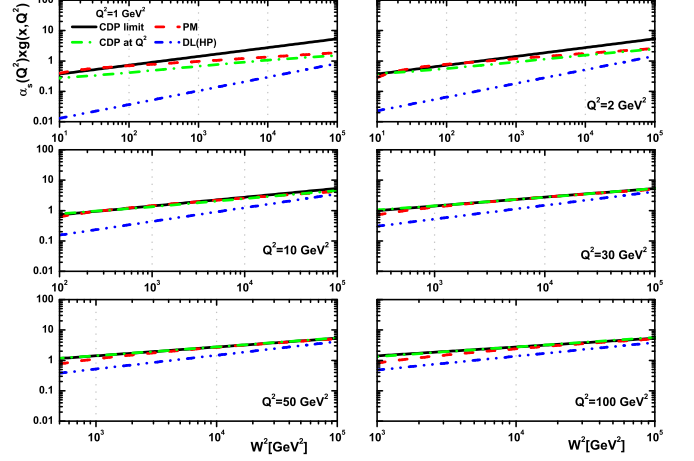


FIG. 4: Same as Fig.3, and compared with hard Pomeron model (HP,Eq.23) (dashed-dot-dot curve).

Pomeron results for $Q^2 > 100 \text{ GeV}^2$. In summary two Pomeron models (soft+hard) improve results in comparison with the CDP and parametrization models at $1 \text{ GeV}^2 \leq Q^2 \leq 100 \text{ GeV}^2$. Soft and hard Pomeron models already discussed in Ref.[31]. The inclusive electroproduction on the proton using a soft and a hard Pomeron have been studied in Ref.[31].

The derivative of the hard-Pomeron behavior from the eye-ball fit can be improved again by considering the tensor-Pomeron behavior of the proton structure function in Fig.4. In Ref.[30] the soft and hard Pomeron coupling functions are obtained for $Q^2 = 10$ and 50 GeV^2 . Therefore in Fig.5 we show that results obtained in Fig.4 are comparable with others as we used the tensor-Pomeron approach of the proton structure function. According to (25), the gluon distribution may equivalently be expressed in terms of the structure function due to the tensor-Pomeron approach. As seen in Fig.5, the results at $Q^2 = 10$ and 50 GeV^2 are comparable with others. The results obtained by employing the tensor-Pomeron approach are comparable with CDP representation than the hard-Pomeron approach.

To conclude the low- x analysis one needs the explicit expressions for the gluon distribution, $xg(x, Q^2)$, in Eq.(12) as

$$xg(x, Q^2) = \frac{3\pi}{\alpha_s(Q^2) \sum e_q^2 (2\rho + 1)} F_2(\xi_L x, Q^2), \quad (26)$$

where the proton structure functions are defined in Eqs.(14), (16), (21) and (24) according to the CDP [5,7,23], PM [9], DL [28] and TP [30] models respectively. With the explicit form of the standard representation for QCD couplings at the LO and NLO approximations in Eq.(5), the behavior of gluon distribution is investigated.

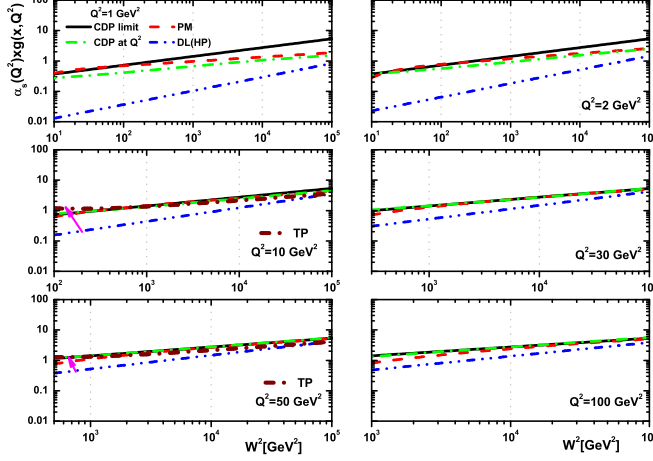


FIG. 5: Same as Fig.4. The tensor-Pomeron (TP) behavior of the proton structure function plotted at $Q^2 = 10$ and 50 GeV^2 (TP, Eq.25) (short-dash-dot curve).

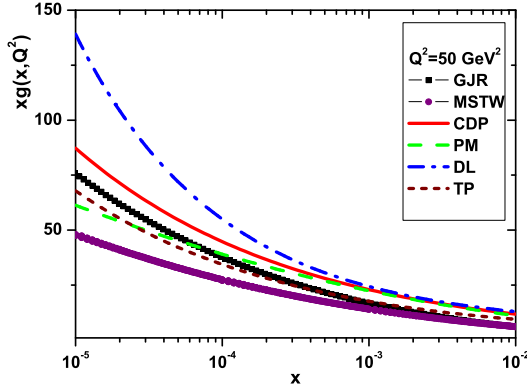


FIG. 6: The gluon distributions for $Q^2 = 50 \text{ GeV}^2$ by using the CDP [5,7,23], PM [9], DL [28] and TP [30] models compared to the GJR [33] and MSTW [34] parameterizations.

In Ref.[32] the authors defined the renormalization group equations of the QCD running coupling and quark masses in a mathematically strict way. The QCD scale parameter Λ has been extracted from the running coupling α_s normalized at the Z -boson mass, $\alpha_s(M_Z^2)$, where $\Lambda_{\text{LO}}^{n_f=4} = 119 \text{ MeV}$ and $\Lambda_{\text{NLO}}^{n_f=4} = 322 \text{ MeV}$. We have calculated the x -dependence of the gluon distribution function as described above in the NLO approximation. In Fig.6, we present the comparison of the gluon distribution from the CDP [5,7,23], PM [9], DL [28] and TP [30] models, with the results based on the GJR [33] and MSTW [34] parameterizations at $Q^2 = 50 \text{ GeV}^2$. As can be seen, the values of the gluon distribution function

increase as x decreases. This figure indicates that the obtained results from the present analysis, based on the CDP are compatible with the ones obtained from the parametrization methods.

4. Conclusion

In conclusion, we have studied the effects of soft and hard Pomeron in relation to the CDP and Parametrization models. We determined the gluon distribution function (multiplied by $\alpha_s(Q^2)$) from our representation of the photoabsorption cross section in the CDP and compared with the results of the parametrization of the proton structure function and the soft and hard Pomeron in the structure function of the proton. It turned out that the gluon function at order $\alpha_s(Q^2)$ is proportional to the proton structure function at a shifted scale $x \rightarrow \xi_L x$. The parametrization and CDP results have similar behavior at $10 \text{ GeV}^2 \leq Q^2 \leq 100 \text{ GeV}^2$. We have found that the Regge like behavior of the proton structure function with a soft and hard Pomeron and also tensor-Pomeron approach improve the description of the gluon behavior at $10 \text{ GeV}^2 \leq Q^2 \leq 100 \text{ GeV}^2$. The soft and hard Pomeron results confirm the predictions of the CDP and this is requiring consistency of the CDP and pQCD for $Q^2 \gtrsim 10 \text{ GeV}^2$.

Furthermore, we have shown that the gluon distribution from the proton structure function can be estimated with respect to the running coupling in a general model using the CDP model. Explicit, analytical expressions for the gluon distribution function are obtained in terms of the effective parameters of the proton structure function in CDP, PM, DL and TP models and results of numerical calculations as well as comparisons with GJR and MSTW parametrizations are presented.

ACKNOWLEDGMENTS

The author is grateful to Razi University for the financial support of this project.

REFERENCES

1. J.J.Sakurai and D.Schildknecht, Phys.Lett.B40, 121(1972); B.Gorczyca and D.Schildknecht, Phys.Lett.B47, 71(1973).
2. N.N.Nikolaev and B.G.Zakharov, Z.Phys.C49, 607(1991); N.N.Nikolaev and B.G.Zakharov, Z.Phys.C53, 331(1992).
3. K.Golec-Biernat and M.Wüsthoff, Phys.Rev.D59,

TABLE I: The effective parameters at low x are defined by the Block-Halzen fit to the real photon-proton cross section as $M^2 = 0.753 \pm 0.068 \text{ GeV}^2$, $\mu^2 = 2.82 \pm 0.290 \text{ GeV}^2$, $n = 11.49 \pm 0.99$ and $\lambda = 2.430 \pm 0.153$ [9].

parameters	value
a_{10}	$8.205 \times 10^{-4} \pm 4.62 \times 10^{-4}$
a_{11}	$-5.148 \times 10^{-2} \pm 8.19 \times 10^{-3}$
a_{12}	$-4.725 \times 10^{-3} \pm 1.01 \times 10^{-3}$
a_{20}	$2.217 \times 10^{-3} \pm 1.42 \times 10^{-4}$
a_{21}	$1.244 \times 10^{-2} \pm 8.56 \times 10^{-4}$
a_{22}	$5.958 \times 10^{-4} \pm 2.32 \times 10^{-4}$
a_{00}	$2.550 \times 10^{-1} \pm 1.600 \times 10^{-2}$
a_{01}	$1.475 \times 10^{-1} \pm 3.025 \times 10^{-2}$

014017(1998); H.Kowalski, L.Motyka and G.Watt, Phys.Rev.D**74**, 074016(2006).
4. M.R.Pelicer et al., Eur.Phys.J.C**79**, 9(2019); B.Sambasivam, T.Toll and T.Ullrich; Phys.Lett.B**803**, 135277(2020); G.M.Peccini, F.Kopp, M.V.T.Machado and D.A.Fagundes, Phys.Rev.D**101**, 074042 (2020).
5. M.Kuroda and D.Schildknecht, Phys.Lett. B**618**, 84(2005); M.Kuroda and D.Schildknecht, Phys.Rev. D**96**, 094013(2017); D.Schildknecht, B.Surrow and M.Tentyukov, Eur.Phys.J.C**20**, 77(2001); M.Kuroda and D.Schildknecht, International Journal of Modern Physics A**31**, No. 30, 1650157 (2016); G.Cvetič, D.Schildknecht and A.Shoshi, Eur.Phys.J.C**13**, 301(2000); D.Schildknecht, Nuclear Physics B Proceedings Supplement**00**,1 (2012);
6. C.Ewerz, A.von Manteuffel and O.Nachtmann, JHEP**03**, 102(2010); C.Ewerz, A. von Manteuffel and O.Nachtmann, Phys.Rev.D**77**, 074022(2008).
7. M.Kuroda and D.Schildknecht, Phys.Rev.D**85**, 094001(2011).
8. M. M. Block and L. Durand, arXiv [hep-ph]: 0902.0372 (2009).
9. M. M. Block, L. Durand and P. Ha, Phys. Rev.D**89**, 094027 (2014).
10. J.Breitweg et al. (ZEUS), Phys.Lett.B**487**, 53(2000); S.Chekanov et al. (ZEUS), Eur.Phys.J.C**21**, 443(2001).
11. E.L.Berger, M.M.Block and C.-I.Tan, Phys.Rev.Lett.**98**, 242001(2007).
12. M.M.Block, Nucl.Inst. and Meth.A**556**, 308(2006).
13. R.G.Roberts, The structure of the proton:Deep inelastic scattering, Cambridge University Press (1990).
14. A.D. Martin et al., Phys. Rev. D**37**, 1161(1988);

A.M. Cooper-Sarkar et al., Z. Phys. C**39**, 281(1988); A.M. Cooper-Sarkar et al., Acta Phys.Pol.B**34**, 2911(2003).
15. G.R.Boroun and B.Rezaei, Eur.Phys.J.C**72**, 2221(2012).
16. H.D.Politzer, Phys.Rev.Lett. **30**, 1346 (1973); D.J Gross and F.Wilczek, Phys.Rev.Lett. **30**, 1343 (1973); W.A.Caswell, Phys.Rev.Lett. **33**, 244 (1974).
17. O.V.Tarasov, A.A.Vladimirov and A.Yu.Zharkov, Phys.Lett.B **93**, 429 (1980); S.A.Larin and J.A.M.Vermaseren, Phys.Lett.B **303**, 334 (1993); R.K.Ellis, W.J.Stirling and B.R.Webber, "QCD and Collider Physics", Cambridge university press, (1996).
18. J.Österman, arXiv [math-ph]: 1912.08016.
19. L.N. Lipatov, Sov. J. Nucl. Phys.**20**, 94(1975); V.N. Gribov, L.N. Lipatov, Sov. J. Nucl. Phys.**15**, 438 (1972); G. Altarelli, G. Parisi, Nucl. Phys. B**126**, 298(1977); Yu.L. Dokshitzer, Sov. Phys. JETP **46**, 641 (1977).
20. K. Prytz, Phys. Lett. B **311**, 286(1993).
21. G.R.Boroun, Phys.Rev.C**97**, 015206(2018).
22. G.R.Boroun and B.Rezaei, Eur.Phys.J.C**73**, 2412(2013).
23. D.Schildknecht, arXiv [hep-ph]:1104.0850 (2011).
24. G.R.Boroun, Eur.Phys.J.A **57**, 219 (2021).
25. L.P.Kaptari et al., Phys.Rev.D**99**, 096019 (2019).
26. G.R.Boroun and B.Rezaei, Phys.Rev.C **103**, 065202 (2021).
27. C.Adloff et al.[H1 Collab.], Phys.Lett.B**520**, 183 (2001).
28. P.V.Landshoff, arXiv [hep-ph]:0203084 (2002); A.Donnachie and P.V.Landshoff, Phys.Lett.B**595**, 393 (2004); A.Donnachie and P.V.Landshoff, Phys.Lett.B**533**, 277 (2002); A.Donnachie and P.V.Landshoff, Phys.Lett.B**550**, 160 (2002).
29. D.Schildknecht, Phys.Rev.D **104**, 014009 (2021); G.R.Boroun, M.Kuroda and D.Schildknecht, arXiv [hep-ph]: 2206.05672.
30. D.Britzger, C.Ewerz, S.Glazov, O.Nachtmann and S.Schmitt, Phys.Rev.D **100**, 114007 (2019).
31. J.R.Cudell, A.Lengyel, E.Martynov and O.V.Selyugin, Nucl.Phys.B Proc.Suppl. **152**, 79 (2006); arXiv [hep-ph]: 0710.5391; U.D'Alesio, A.Metz and H.J.Pirner, Eur.Phys.J.C **9**, 601(1999).
32. H.M.Chen et al., International Journal of Modern Physics E**31**, No.02, 2250016 (2022).
33. M. Gluck, P. Jimenez-Delgado, E. Reya, Eur.Phys.J.C **53**, 355 (2008).
34. A. Martin, W. Stirling, R. Thorne, and G. Watt, Eur.Phys.J. C **63**, 189 (2009).